Title: Semi-automated protocol to quantify and characterize fluorescent, 3D vascular images

Danny F. Xie[1,2], Christian Crouzet[1,2], Krystal LoPresti[1,2], Yuke Wang[1,2], Christopher Robinson[1,2], William Jones[1,2], Fjolla Muqolli[1,2], Alessandria Pai[1,2], Chuo Fang[3], David H. Cribbs[4], Mark Fisher[1,2,3,4,5], and Bernard Choi[1,2]

Affiliations:
[1]Beckman Laser Institute and Medical Clinic, University of California-Irvine, Irvine, CA, USA
[2]Department of Biomedical Engineering, University of California-Irvine, Irvine, CA, USA
[3]Department of Neurology, University of California-Irvine, Irvine, CA, USA
[4]Institute for Memory Impairments and Neurological Disorders, University of California-Irvine, Irvine, CA, USA
[5]Department of Pathology & Laboratory Medicine, University of California-Irvine, Irvine, CA, USA

ABSTRACT

The microvasculature facilitates gas exchange, provides nutrients to cells, and regulates blood flow in response to stimuli. Vascular abnormalities are an indicator of pathology for various conditions, such as compromised vessel integrity in small vessel disease and angiogenesis in tumors. Traditional immunohistochemistry enables visualization of tissue cross-sections containing exogenously labeled vasculature. Although this approach can be utilized to quantify vascular changes within small fields-of-view, it is not a practical way to study the vasculature on the scale of whole organs. Three-dimensional (3D) imaging presents a more appropriate method to visualize the vascular architecture in tissue. Here we describe the complete protocol that we use to characterize the vasculature of different organs in mice encompassing the methods to fluorescently label vessels, optically clear tissue, collect 3D vascular images, and quantify these vascular images with a semi-automated approach. To validate the automated segmentation of vascular images, one user manually segmented fifty random regions of interest across different vascular images. The automated segmentation results had an average sensitivity of 80±8% and an average specificity of 90±5% when compared to manual segmentation. Applying this procedure of image analysis presents a method to reliably quantify and characterize vascular networks in a timely fashion. This procedure is also applicable to other methods of tissue clearing and vascular labels that generate 3D images of microvasculature.

INTRODUCTION

The microvasculature facilitates gas exchange, provides nutrients to cells, and regulates blood flow in response to stimuli. Thus, it plays a fundamental role in the survival and health of tissues and organs. Vascular abnormalities are an indicator of pathology for various conditions, such as compromised vessel integrity in small vessel disease and angiogenesis in tumors (Carmeliet & Jain, 2011; Haller et al., 2018). In addition, impaired blood flow to the brain is associated with neurodegenerative diseases such as Alzheimer's disease (Sweeney et al., 2018).

Traditional immunohistochemistry enables visualization of tissue cross-sections containing exogenously labeled vasculature. Although this approach can be used to quantify vascular changes within small fields-of-view, it is not a practical way to study the vasculature on the scale of whole organs. Furthermore, traditional immunohistochemistry requires the sectioning of tissue into thin (6-40 μm) sections, which effectively limits visualization of features to planar views and thus impedes facile 3D visualization of vascular architecture.

Volumetric imaging of tissue samples is vital to studying the microvasculature in its

native state. The main limitation to 3D imaging of tissue samples is optical scattering resulting from the microscopic variations of refractive index occurring in most biological tissues. Organic solvents and aqueous solvents have been used to reduce tissue turbidity by achieving refractive index matching (Renier et al., 2014; Susaki et al., 2014). CLARITY is a popular method used for tissue clearing that involves embedding of the sample into a hydrogel and using an electric current to remove lipids from the sample (Chung et al., 2013). Other tissue clearing procedures have advantages and disadvantages associated with clearing time, extent of clearing, and preservation of original tissue characteristics (size, endogenous fluorescence, etc.).

Quantitative analysis of microvasculature is essential to understand how structural variations in the microvascular network may change for different pathological states (Kalaria et al., 2016). The feasibility of such analysis depends on accurate, ideally automated segmentation methods for isolating the microvasculature from the background due to the hundreds of gigabytes of data generated with high-resolution 3D imaging. Various groups have developed automated algorithms to perform quantitative characterization of vascular images (Kirst et al., 2020; Moy et al., 2014). Each method varies in complexity, processing time, and computational requirements.

We currently use iDISCO (immunolabeling-enabled three-dimensional imaging of solvent-cleared organs) as our primary method of tissue clearing (Khouri et al., 2021; Renier et al., 2014). Briefly, iDISCO consists of methanol dehydration, lipid removal with dichloromethane, and refractive index matching with dibenzyl ether. iDISCO is a fast, simple-to-implement clearing method that enables deep-tissue imaging. It is compatible with many exogenous labels often used for traditional immunohistochemistry. We previously demonstrated the effectiveness of iDISCO in combination with lectin-DyLight-649 for 3D visualization of vasculature in a mouse brain (Khouri et al., 2021). We also have used Prussian blue labelling of hemosiderin (Crouzet et al., 2021; Lo et al., 2016; Sumbria et al., 2018), a by-product of cerebral microhemorrhages, with iDISCO-cleared brains and lectin-DyLight-649 labelling.

In this paper, we first review different methods for vascular labeling in conjunction with optical clearing that have been published by other groups. Next, we describe the complete protocol that we use for imaging the vasculature in different organs in mice. Specifically, we report on sample collection and perfusion of lectin-DyLight-649 followed by application of additional labels as desired and optical clearing. We then describe our procedure to obtain 3D confocal microscopy images. Finally, we describe our semi-automated approach to process the resulting images and quantify the vascular architecture in three dimensions.

Vascular imaging with various vessel labels and optical clearing techniques

Through reviewing the literature on 3D vascular imaging of cleared tissue, one will quickly realize the large variability in methodology across different experiments (see Table 1 for specific references). For example, blood vessels can be visualized with transgenic animals expressing a fluorescent protein in endothelial cells, labeled *in vivo* with intravascular dyes, or labeled *ex vivo* with immersion-based antibody labelling. In addition, tissue preparation can vary from thick tissue sections and whole organs to whole-mount specimens, depending on the purpose of an experiment. Finally, clearing procedures can be grouped into aqueous solvents (Fu & Tang, 2010; Hama et al., 2015; Loren et al., 2019; Nehrhoff et al., 2017; Nishimura et al., 2018; J. Zhu et al., 2020), organic solvents, and hydrogel-based.

When selecting a clearing procedure, it is essential to consider its compatibility with the chosen vascular label. Endogenous fluorescence intensity is known to be reduced when using the iDISCO protocol; hence, an alternative vascular label would be preferred. Imaging of cleared samples is typically performed with confocal microscopy or light-sheet microscopy. Lastly, vascular-related metrics, such as vessel diameters and vessel density, are quantified with existing software such as FIJI and Imaris, or custom-designed software such as ClearMap 2.0.

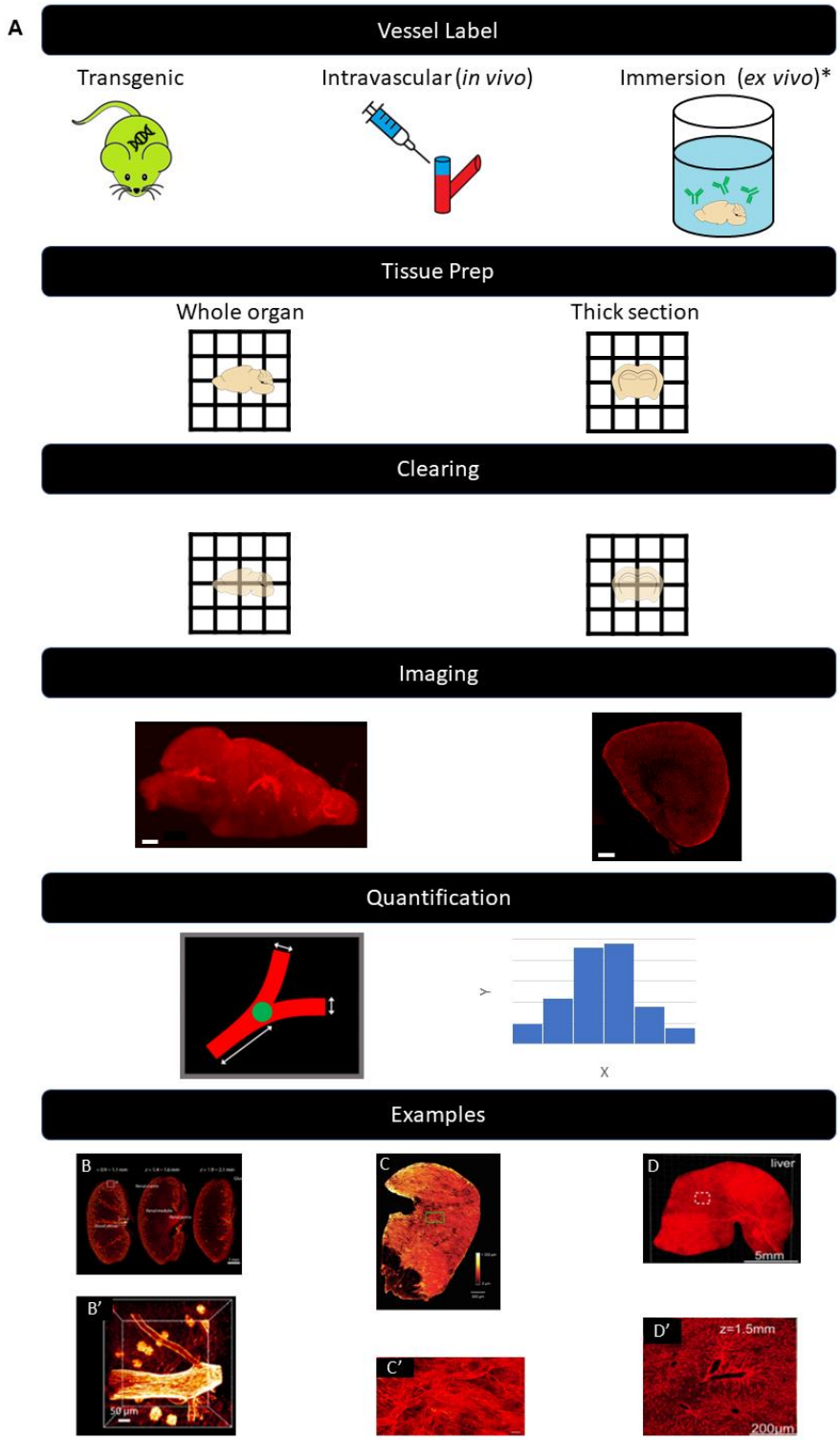

Figure 1. A) Illustrations of the critical steps and workflow for vascular visualization in cleared tissue. B-D) Examples of vascular visualization in literature. B) Visualization of CD31-labeled mouse kidney vasculature with FDISCO (Qi et al., 2019). B') Magnified view of 1B. C) Visualization of DiI-labeled mouse heart vasculature with FocusClear (Moy et al., 2014). C') Magnified view of 1C. D) Visualization of liver vasculature from *Tie2-Cre* mouse model with PEGASOS (Jing et al., 2018). D') Magnified view of 1D).

We have reviewed several optical clearing methods utilized to image vasculature. They are organized in Table 1 by clearing method, tissue type, vessel label, and quantification. Vascular images in cleared tissue from select publications are included in Figure 1B-D. FDISCO is an organic solvent-based clearing method derived from the 3DISCO method. In developing FDISCO, Qi *et al.* found that they could achieve superior fluorescent signals of CD31-labelled vessels by optimizing temperature and pH conditions (Figure 1B, 1B') (Qi et al., 2019; White et al., 2011). Moy *et al*. visualized vessels with an intravascular fluorescent dye along with FocusClear (Figure 1C, 1C') (Moy et al., 2014). They were able to quantify functional vascular density in different regions of cardiac tissue with a custom MATLAB algorithm (White et al., 2011). With a polyethylene glycol-associated solvent system (PEGASOS), researchers developed a clearing technique that preserved both hard and soft tissue structures (Figure 1D, 1D') (Jing et al., 2018), allowing for vascular imaging throughout an entire specimen.

Table 1. Summary of different approaches to visualize 3D microvasculature in optically cleared tissues.

Clearing agent(s)	Organ(s)	Vascular label	Quantification Method/Tool	Quantified Metrics
MACS (J. Zhu et al., 2020)	brain, heart, lung, spleen, femur, kidney, spinal cord, embryo, entire body	DiI, tetramethylrhodamine-conjugated dextran	Custom algorithm via Python, Imaris: surface function	glomerulus number and glomerulus volume; general metrics (imaging depth, size change, fluorescence intensity)
SeeDB, SeeDB2, 3DISCO, uDISCO, iDISCO, CUBIC, simplified CLARITY method, 75% v/v glycerol, Ce3D, FRUIT (Matryba et al., 2020)	lymph nodes	CD31	Imaris: surface function, ImageJ	general metrics (imaging depth, size change, fluorescence intensity)
sodium dodecyl sulfate/sodium deoxycholate with Sca*l*eCUBIC-2 (Miyawaki et al., 2020)	brain	RITC-Dex-GMA, Texas red lectin, CD31, αSMA	N/A	capillary diameters, signal-to-noise ratio
iDISCO (Renier et al., 2014)	brain, peripheral nervous system, kidney, muscle, heart, whisker pad, entire embryo	PeCAM	N/A	N/A
iDISCO with CUBIC (McKey et al., 2020)	ovary	endomucin	N/A	N/A
FDISCO (Qi et al., 2019)	brain, kidney	AlexaFluor647, CD31, lectin-DyLight-649	Imaris, ImageJ	general metrics (size change, imaging depth, fluorescence quantification)
Sca*l*eS (Hama et al., 2015)	brain	Texas Red lectin	custom C++, commercial Volocity, commercial Igor Pro	microglia and Aβ plaques with custom C++, distance between microglia and Aβ plaques
3DISCO (Lugo-Hernandez et al., 2017)	brain	FITC albumin-gelatin hydrogel	Imaris, ImageJ	vessel density, vessel diameter
thiazone with PEG-400 (D. Zhu et al., 2010)	dorsal skin	N/A (imaged blood flow via LSI)	N/A	bloodflow via LSCI

iDISCO (Liebmann et al., 2016)	brain	Dye-conjugated secondary antibodies	ClearMap	Aβ deposits
CLARITY, TDE (Di Giovanna et al., 2018)	brain	lectin-FITC, gel-BSA-FITC, gel-BSA-TRITC	Markov random field based algorithm, ImageJ, Amira 5.3 software	automatic segmentation, vessel diameter, vessel length
FACT (Khoradmehr et al., 2019)	brain, spinal cord, heart, lung, adrenal gland, pancreas, liver, esophagus, duodenum, jejunum, ileum, muscle, bladder, ovary, uterus	CD31, auto fluorescence	Imaris	segmentation
CUBIC, BABB (Nehrhoff et al., 2017)	heart	FITC-lectin, 649-lectin, CD31	N/A	N/A
BABB (Ivins et al., 2016)	heart	PECAM1	N/A	N/A
DBE, SCALE, CLARITY, CUBIC (Kolesová et al., 2016)	heart and embryo	GFP		
vDISCO (Cai et al., 2019)	whole mouse	GFP, lectin	ImageJ, ClearMap	signal level, microglia distribution
3DISCO (Harrison et al., 2018)	brain	tomato lectin	N/A	N/A
CLARITY (Krolewski et al., 2018)	brain	fluorescein-conjugated tomato lectin	Amira	area, volume, perimeter, and length of stained vessel
CLARITY with ScaleA2 (Oren et al., 2018)	ovary, uterus, lung, liver	tdTomato	Ilastik, Imaris	segmentation, total vessel length, vessel mean diameter, vessel straightness, total number of branching points
PEGASOS (Jing et al., 2018)	whole mouse	αSMA, GS-IB4 isolectin dye, collagen IV	Imaris	vessel density
iDISCO (Kirst et al., 2020)	brain	CD31, podocalyxin, collagen IV, smooth muscle actin, transgelin, von Willebrand factor	ClearMap 2.0, TubeMap	vascular density, vascular orgnaization, vascular remodeling

ethyl-cinnamate (Huang et al., 2019)	liver, skin, lung, heart, muscles, pancreas, brain, kidney	In-house developed NIR fluorescent dye (MHI148-PEI)	Leica LAS X	segmentation, volume of glomerulus
X-CLARITY (Carrillo et al., 2018)	placenta	DiI	Imaris, Image-Pro Premier	N/A
CLARITY, iDISCO (Lagerweij et al., 2017)	brain	lectin-DyLight, lectin-FITC, anti-CD31	Imaris, segmentation	number of branches, total vessel length, total vessel volume, total vessel area, diameter of single segments per volume, distance between cells and nearest vessel
PEGASOS (Yi et al., 2019)	bone, teeth	tdTomato	Imaris	blood vessel volume
Sca*l*eS (Nishimura et al., 2018)	pancreas	lectin-DyLight	N/A	N/A
CLARITY (Singh et al., 2017)	retina	Griffonia lectin	Angiotool, ImageJ, Vaa3D, MATLAB, APP-2.0	network tracing, vessel percentage area, total number of junctions, junction density, total vessel length, average vessel length, total number of endpoints, mean lacunarity
No clearing approach (Y. Li et al., 2008)	retina, heart	DiI	N/A	N/A
FocusClear (Fu & Tang, 2010)	small intestine	DiI	N/A	N/A
FocusClear, ScaleSQ, RIMS, sRIMS (Loren et al., 2019)	brain	Lectin-Dylight649	MATLAB	optical properties, vascular density
FRUIT 100 (Peviani et al., 2020)	brain tumor	DiI	N/A	N/A
FocusClear (Moy et al., 2015)	brain	DiI	N/A	optical properties
FocusClear (Moy et al., 2013)	brain	DiI	MATLAB	functional vascular density

Three-dimensional quantitative analysis of microvasculature imaged in thick tissue sections

Microvascular labeling is performed with an injection of a lectin conjugated to a fluorophore. In our work, we have focused on the DyLight-649 fluorophore. As the lectin travels through the circulatory system, it binds to glycoproteins adjacent to endothelial cells of the vascular wall. This binding allows for labeling of the vascular network within every organ of the body.

An overview of our workflow is outlined below in Figure 2. We administer lectin-DyLight-649 via retroorbital injection. The lectin is allowed to circulate throughout the body prior to cardiac perfusion with saline followed by formalin. Mouse brains are then extracted, bisected into hemispheres, and sectioned into thick (0.5-1.0mm) sections. Each section is then imaged using confocal microscopy to generate image stacks of the complete section throughout its entire thickness. Segmentation is performed by a custom MATLAB (MathWorks, Natick, MA) script. Finally, neuTube, an open-source neuron tracing software, is used to extract diameter measurements of the vessel structures (Feng et al., 2015). Below, we describe in detail the materials and methods we use.

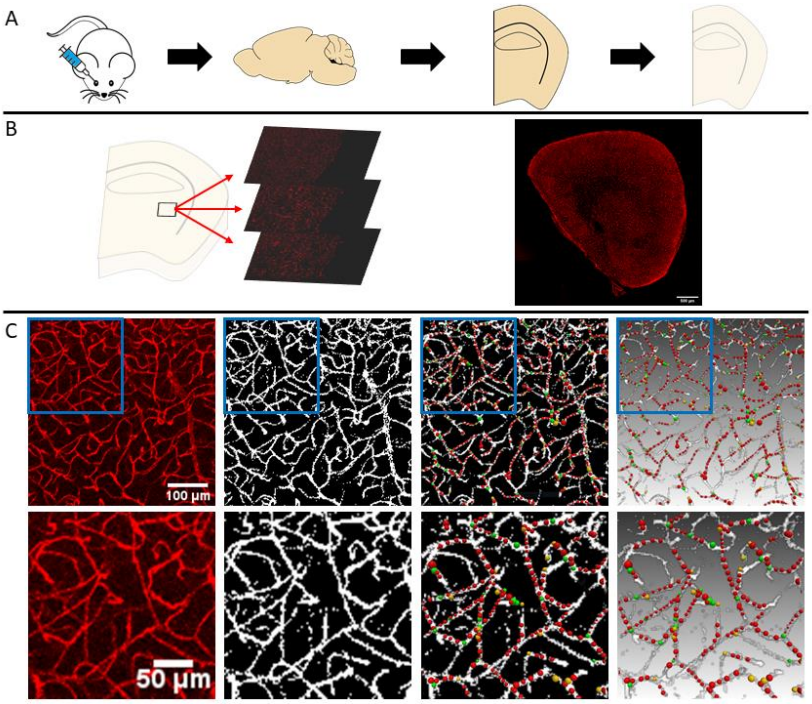

Figure 2. Workflow for 3D visualization and quantitation of microvasculature in thick tissue sections. A) Vasculature is labeled via retroorbital injection of lectin-DyLight-649. Brains are then sectioned and cleared. B) Depiction of z-stack imaging and tile stitching to visualize an entire sample in 3D via confocal microscopy. C) From left to right: representative example of a raw image of the vasculature, segmented vasculature via MATLAB, and traced vasculature via neuTube.

METHODS

Equipment and supplies

Reagents:

- Saline solution (Aspen Veterinary Resources, NDC No. 46066-807-50)
- 10% formalin solution (Sigma-Aldrich Product Code HT50-1-1)
- PBS with 0.02% sodium azide solution (Syringa Lab Supplies, Part No. 11001)

- Potassium ferrocyanide (Sigma: P3289-500G)
- Hydrochloric acid (Fisher: A144-212)
- Methanol (Fisher: A412S)
- Deionized water
- Dichloromethane (Sigma: 270997-100ML)
- Dibenzyl ether (Sigma: 108014-1KG)

Equipment:

- 2x 10 mL syringes (Sigma-Aldrich: Z683604)
- 1x 23G x ¾ x 12" butterfly needle (Vaculet, 26766)
- 3x hemostat clamps (Excelta: 37SE)
- 1x bone scissors (Fine Science Tools: 91604-09)
- 1x forceps (Fine Science Tools: 11000-12)
- 1x scissors (Excelta: 290)
- 1x angled scissors (Fine Science Tools: 15010-10)
- 1x spatula (Fine Science Tools: 10089-11)
- 1x syringe pump (Harvard Apparatus Model 11 Plus)
- 1x 20 mL glass scintillation vial (Grainger: 3LDT2)
- Aluminum foil
- Tape
- Liquid absorbent mats
- Isoflurane chamber (E-Z Systems: EZ-178)
- Nose cone (E-Z Systems: EZ-103A)
- Magnetic stir plate with stir bar (Corning PC 353 Stirrer)
- Orbital shaker (Scilogex: SK-D1807-E)
- Scale
- Weigh boats
- Pipette controller (Grainger: 49WF85)
- Serological pipette tips
- 1.5 mL opaque microcentrifuge tube (Argos Technologies: 06333-80)
- Microcentrifuge tube rack
- Pipettes
- 18-gauge needle
- Leica TCS SP8 microscope

Software:

- MATLAB (https://www.mathworks.com/)
- FIJI (https://imagej.net/Fiji)
- neuTube (https://www.neutracing.com/)

Reagent setup:

- *10% potassium ferrocyanide (PF) solution*
  - Dissolve the appropriate amount of PF in deionized water (DIW) (10 g of PF per 100 mL of DIW) to create a 10% PF solution. Use a magnetic stir bar and magnetic stir plate to dissolve potassium ferrocyanide.
- *20% hydrochloric acid (HCl) solution*
  - Dilute the appropriate amount of stock HCl solution in DIW (20 mL of stock HCl per 80 mL of DIW) to create 20% HCl solution. Perform this step under a fume hood.
- *Potassium ferrocyanide/hydrochloric acid working solution*
  - Mix 1 part 10% potassium ferrocyanide solution per 1 part 20% HCl solution

Cardiac perfusion protocol and sample preparation

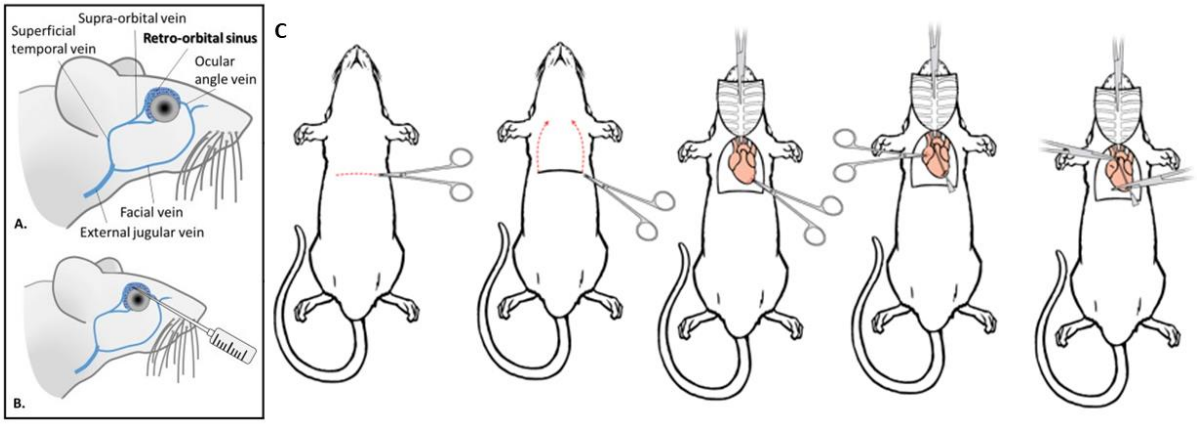

Figure 3. Key steps for animal procedures. A,B) Retroorbital injection diagram. Correct needle placement is shown. C) Incision points for opening the chest cavity. A lateral incision beneath the diaphragm and a vertical incision along both sides of the chest opens the chest cavity. The right atrium of the heart is cut, and a needle is inserted into the left ventricle (Gage et al., 2012; Prabhakar et al., 2021).

Cardiac perfusion

Begin by anesthetizing a mouse using an isoflurane chamber with 1.5 L/min of oxygen and 4.0% isoflurane. Once the mouse is anesthetized, remove it from the chamber and place its snout in a nose cone at 1.5 L/min oxygen and 1.5% isoflurane. Administer a solution of lectin-DyLight-649 (200 µL, 25% lectin-DyLight and 75% saline) via retroorbital injection (see Figure 3A,B) (Gage et al., 2012; Yardeni et al., 2011). Allow the solution to circulate for about 20 minutes before proceeding with the cardiac perfusion (Robertson et al., 2015).

It is recommended to perform the cardiac perfusion on a surgical tray or similar platform to contain the exsanguinated blood. Confirm that the mouse is at an appropriate plane of anesthesia using toe and/or tail pinches. Next, open the chest cavity by performing a horizontal incision beneath the rib cage and a vertical incision along both sides of the chest (see Figure 3C) (Gage et al., 2012). Use hemostats to assist with holding the chest open to access the heart. Then, perform a small incision on the right atrium of the heart to allow blood to exit the body. This is followed by inserting a butterfly needle into the left ventricle of the heart. Use a syringe pump to perfuse 10 mL of saline into the heart at a rate of 2 mL/min. Afterwards, perfuse 10 mL of formalin at a rate of 2 mL/min.

Brain extraction

Remove the head by cutting caudal of the skull with scissors (bone scissors or large scissors preferred). Cut the scalp to create two folds and expose the cranium. Using angled microscissors, gently cut upwards from the foramen magnum to approximately the location of bregma on the brain. Using a set of scissors, perform a lateral cut directly rostral to the olfactory bulbs. This cut should split the remainder of the skull down the centerline beyond bregma. Use fine tweezers or a spatula to pry open each hemisphere of the skull. Gently separate the brain from the base of the skull with a spatula. Sever any nerves connecting the brain to the skull. Place the brain in ~10 mL of 10% formalin to completely submerge the brain. After 24h, store the brain in PBS with 0.02% sodium azide at 4°C until further tissue processing.

(Optional) Exogenous labeling of hemosiderin with Prussian blue for cerebral microhemorrhage visualization

The following procedures are based on 1-mm thick coronal sections of a bisected brain.

Volumes and times may need to be adjusted for tissues of different sizes.

Prepare a working solution of 10% w/v of potassium ferrocyanide (10 g of potassium ferrocyanide per 100 mL of DIW). Use a magnetic stir plate to mix the solution for at least 20 minutes. Next, prepare a working solution of hydrochloric acid that is 20% of stock hydrochloric acid. Mix the solutions of potassium ferrocyanide and hydrochloric acid in a 1:1 ratio. Approximately 5 mL of the mixed solution is used per sample. This solution should be prepared prior to each staining session.

Wash samples in 5 mL of DIW with shaking. Submerge each sample into 5 mL of the working potassium ferrocyanide/hydrochloric acid solution for 1 hour. Afterward, perform a final DIW wash for 5 minutes. Store the samples in PBS with 0.02% sodium azide at 4 C°.

Tissue clearing

The following procedure is modified from the established iDISCO protocols (Renier et al., 2014). Wash durations were modified for 1-mm thick coronal sections of a bisected brain.

Perform a series of methanol washes (20%, 40%, 60%, 80%, 100%, and 100%, balance DIW) each for 20 minutes with shaking. Microcentrifuge tubes of 1.5 mL (or larger for larger samples) are recommended. Fill the tubes fully to minimize exposure to oxygen. Next, incubate the samples in a solution of 66% dichloromethane and 33% methanol for one hour with shaking. The sample may be stored overnight in this situation if desired, without shaking. Next, incubate the sample in dichloromethane twice for 15 minutes with shaking. Lastly, store the samples in dibenzyl ether at 4°C until imaging.

Imaging with confocal microscopy

When imaging samples that have been cleared following the iDISCO protocol, it is recommended to image the sample while submerged in dibenzyl ether. There are various methods to safely house a sample with dibenzyl ether and protect the imaging objective. A straightforward method is to create an epoxy well on a cover glass to surround the sample and hold the dibenzyl ether.

To image the vasculature labeled with the lectin-DyLight-649, use an appropriate wavelength (633 nm can work) with an emission band of approximately 650-750 nm. To visualize microhemorrhages labeled with Prussian blue, locate regions of Prussian blue positivity using a white light source. Simultaneously collect a fluorescent image of the vasculature and a transmittance image to co-register the vascular fluorescence with cerebral microhemorrhages. This workflow along with representative images are depicted in Figure 4.

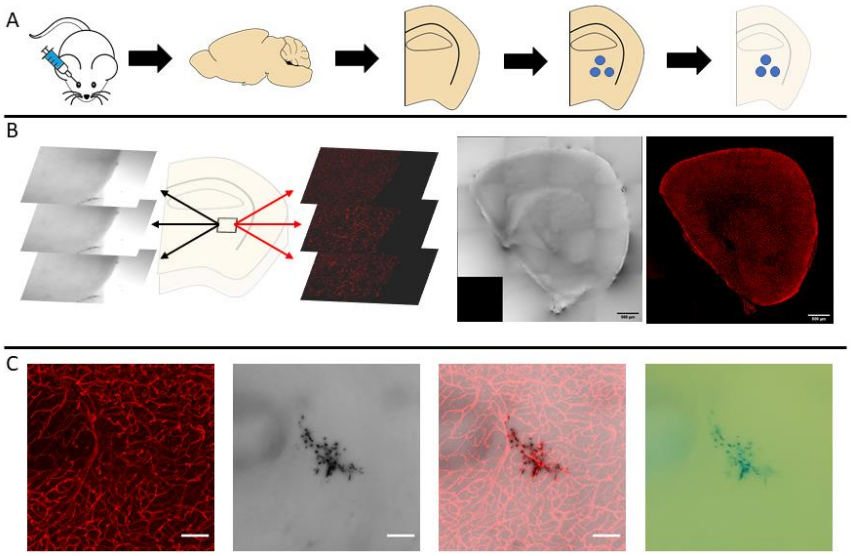

Figure 4. Workflow for 3D visualization of cerebral microvasculature cerebral microhemorrhage in thick tissue sections. A) Vasculature is labeled via retroorbital injection of lectin-DyLight-649. Brains are then sectioned, stained, and cleared. B) Depiction of z-stack imaging and tile stitching for a fluorescence channel and a transmission channel via confocal microscopy. C) From left to right: fluorescent image of microvascular network in a 70 µm thick tissue region, transmission image of cerebral microhemorrhage in the same tissue region, overlayed image of both imaging channels, eyepiece view of Prussian blue positive cerebral microhemorrhage. Scale bars are 100 µm.

In addition to imaging brain microvasculature, the combination of iDISCO and lectin-DyLight-649 enables visualization of the microvascular network of other organs. Light-sheet microscopy can be used as an alternative to confocal microscopy to rapidly generate 3D reconstructions of the vascular network with minimal photobleaching. Figure 5 shows representative images of different labeled and cleared organs imaged with confocal microscopy and light-sheet microscopy.

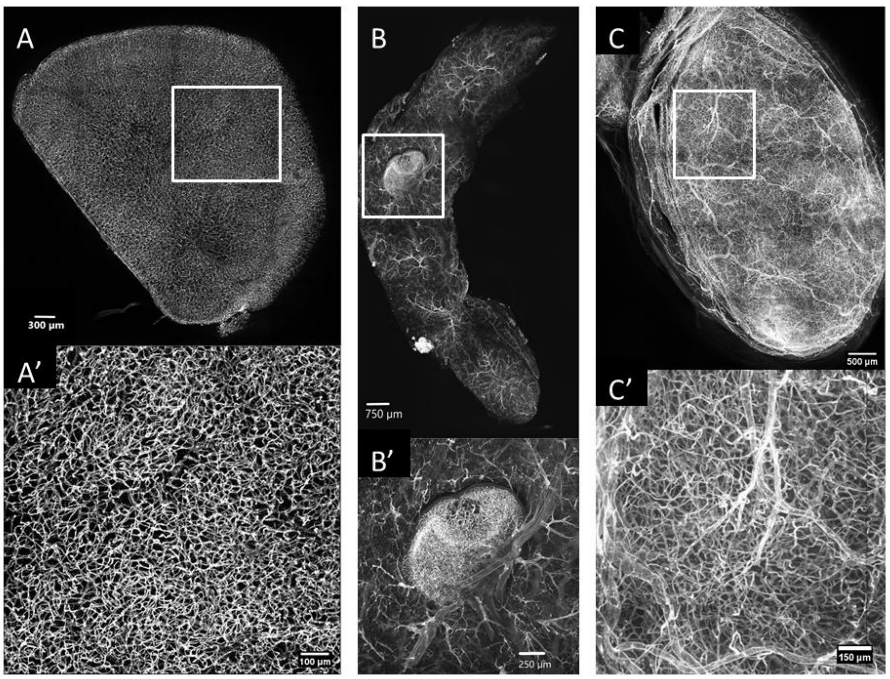

Figure 5. Lectin-DyLight-649 labeling and iDISCO optical clearing enable detailed visualization of mouse organ microvasculature. A) Confocal image of a 1-mm thick coronal hemisection of the brain. A') Magnified view of A. B) Light-sheet image of a mammary gland with a lymph node. B') Magnified view of B. C) Light-sheet image of a bladder. C') Magnified view of C.

Vascular segmentation

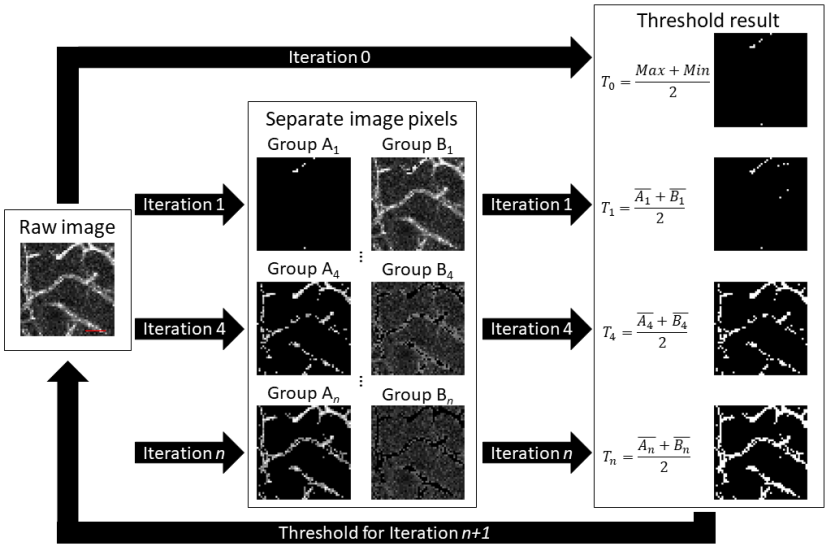

Figure 6. Schematic of iterative selection thresholding method for images of fluorescent vasculature. An initial threshold is selected as the average of the maximum and minimum voxel intensities present in the image. The subsequent iteration assigns voxels to group A_n if a voxel has an intensity greater than the threshold of the previous iteration, or to group B_n if a voxel has an intensity less than the threshold of the previous threshold. Next, the average intensity within each group is calculated, and the average of those two values determines the new threshold. This process is repeated until the change in threshold is less than one intensity value. Scale bar is 25 µm.

There are various segmentation methods to isolate the fluorescent vasculature from the image background. The iterative selection thresholding method was implemented to binarize the fluorescent images (Figure 6) (Ridler & Calvard, 1978). This algorithm was selected due to its simplicity and objectivity and was performed using custom-written code in MATLAB. Vessel parameters such as vascular density and tortuosity can be calculated from the resulting segmented images. An open-source neuron tracing software known as neuTube was used to quantify vessel sizes.

Using MATLAB, a 3x3x1 median filter removes noise within the image data. The iterative selection threshold method is applied by selecting an initial threshold value, T_0. The initial value is the average value of the maximum intensity and the minimum intensity of all voxels of an image.

$$T_0 = \frac{Max + Min}{2}$$

All voxels within an image are separated into two groups: group A_n if a voxel has an intensity equal to or greater than the threshold value of the previous iteration, or group B_n if a voxel has an intensity below the threshold value of the previous iteration.

$$A_n \geq T_n, B_n < T_n$$

The threshold value of the subsequent iteration is calculated as the average value of the

average intensity within groups A_n and B_n.

$$T_n = \frac{\overline{A_n} + \overline{B_n}}{2}$$

This threshold value is compared to the threshold value of the previous iteration. If the difference between the two values is less than 1, the procedure is complete, and the current threshold value is selected. If the difference between the two values is greater than or equal to 1, the procedure repeats for another iteration.

$$If\ |T_n - T_{n-1}| < 1, then\ stop$$

Optional morphological operations can be applied to the resulting binarized image to adjust segmentation results further. The exact parameters for these steps will vary with image acquisition parameters (particularly resolution).

For example, size filtering is performed by removing objects with a volume less than ~50 μm^3 (the exact voxel size will vary based on image resolution) based on an 18-point connectivity scheme. Morphological closing using a spherical structural element with a radius of 1 is applied to close gaps throughout the image. Vascular density can be quantified through built-in MATLAB functions to generate a skeletonized structure, a single-pixel width line along the centerline of vessels, of the vascular image (White et al., 2011). From there, density can be calculated by dividing the total length of the skeleton by a given area. Vessel tortuosity can be calculated by dividing the shortest distance between two endpoints of a vessel and the total length of the vessel (Hart et al., 1999). A complete vessel is defined as the length of the vessel between two branch points.

neuTube tracing to quantify vessel diameters

neuTube is an open-source neuron tracing software that can be applied to tracing tubular structures, such as vasculature (Feng et al., 2015). Automated tracing can be performed on binarized vasculature images in TIF file format. neuTube will output information in an SWC format where tubular structures are simplified into individual nodes with x, y, z coordinates, a radius, and node connectivity information. Each node will be a ‘parent’ to an adjacent ‘child’ node which provides the necessary information to understand how these nodes are connected in space.

Nodal connectivity is used to identify individual vessels based on specific rules. Nodes are defined as branch nodes if they serve as the parent of two different nodes. A node is defined as an end node if it lacks a child node. Individual vessels are defined as a series of nodes bordered by two branch nodes or one branch node and an end node, including the nodes at the borders. The diameter of an individual vessel is defined as the average diameter of all nodes that make up an individual vessel.

Anticipated results

The procedures detailed herein present a simple method for producing optically-cleared (>1-mm thick) tissue samples with fluorescently labeled vasculature. Samples can then be imaged to generate 3D images of the microvasculature. Our presented results are primarily from brain samples, but the procedures can be easily translated to other organs. The described segmentation method using custom MATLAB scripts and neuTube presents an automated method to convert the fluorescent images into binary images. The binary images can then be used to characterize microvasculature by quantifying vessel density and vessel sizes. The procedures here can be enhanced by using additional histology dyes or immunohistochemistry to label biomarkers or other structures of interest in tissue. In doing so, one can visualize and

quantify the microvasculature surrounding these biomarkers to gain insight into their relationship to each other.

Validation

Segmentation results

Manually segmented images were used as a ground truth comparison of automated segmented images. Images from various brain sections across three different animals were used. Each section was imaged by collecting a stack of images that spans the entire thickness of the section. Automated segmentation was performed on each image stack. In addition, manual segmentation was performed on 50 randomly generated ROIs across all images. Each ROI was presented as a maximum intensity projection (MIP) image of a 50x50x5 voxel (113x113x38 µm) region. A MIP is used to present a 2D image that is more feasible for tracing. One author [DFX] was tasked with using MATLAB to outline every object within the image that the author determined to belong to a vessel. The corresponding 50x50x5 voxel region MIP from the automated segmented image was compared. Four representative examples of this are depicted in Figure 7. Across the 50 ROIs, the average sensitivity was 80±8%, and the average specificity was 90±5%. The Dice similarity coefficient between manually segmented and automated segmented images was calculated across all ROIs. This coefficient can measure similarity between two sets of Boolean data and ranges between 0 and 1, where 1 represents identical data, and 0 represents opposite data (Dice, 1945). The average Dice similarity coefficient across 50 ROIs was 0.71±0.07.

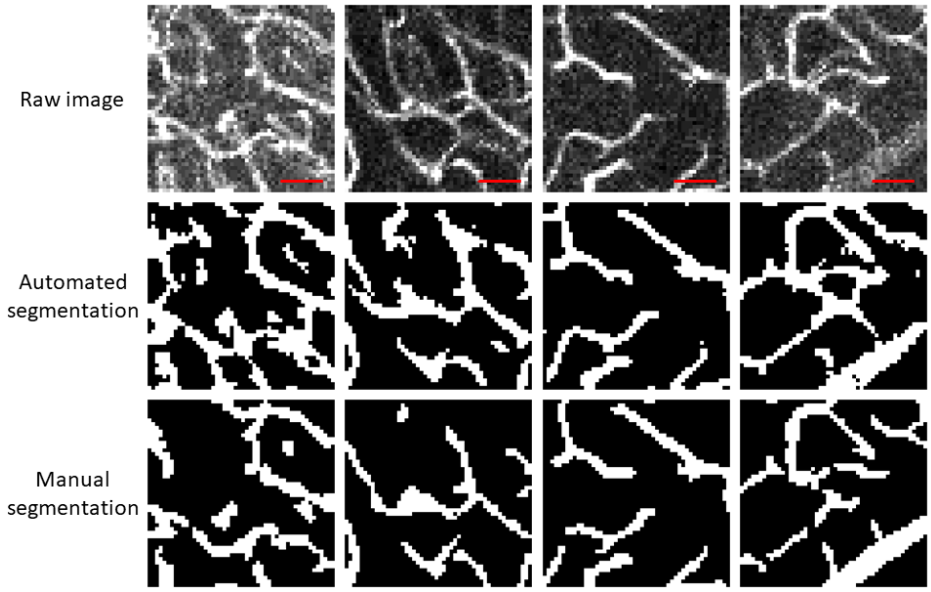

Figure 7. Manual and automated segmentation results. Four examples of different 50x50 pixel regions are shown. Scale bar is 25 µm.

Diameter results with neuTube

Manually measured diameters of individual vessels were used as a ground truth comparison for neuTube approximated vessel diameters. Images from various brain sections across three different animals were used. One author (DFX) was presented with a randomly generated 50x50x5 voxel (113x113x38 µm) size region as a MIP. Within the image, the user was tasked with using MATLAB to estimate the diameter of a single vessel in the image at five different points along the vessel by drawing lines approximately perpendicular to the centerline of the vessel. In neuTube, five nodes along the corresponding vessel were selected. The average of the five manual diameter measurements via MATLAB and the five automated

diameter measurements via neuTube were compared. Two representative examples of this are depicted in Figure 8. The absolute difference between diameter measurements was 1.16±0.73 µm (n=50 vessels of diameters ranging from 1.78 µm to 3.19 µm).

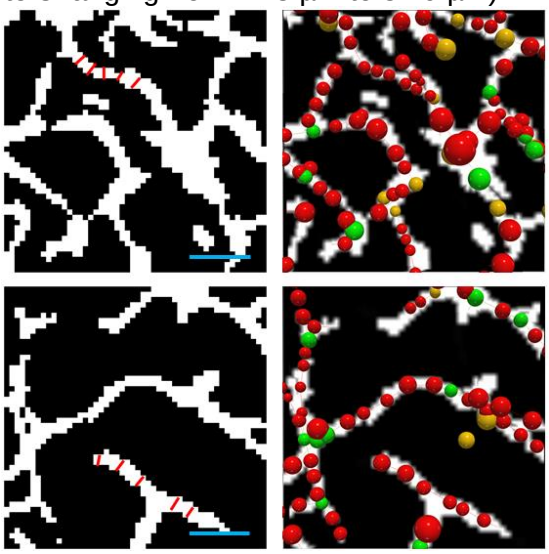

Figure 8. Manual and neuTube diameter results. Two different 50x50 pixel regions are shown, where one vessel is selected for manual measurement. Scale bar is 25 µm.

Potential applications

As angiogenesis occurs in organs, endothelial cells respond to local signals to adapt vessels to the surrounding environment (McDonald, 2008). Angiogenesis plays an essential role in tumor formation. In tumors, angiogenesis directly impacts tumor growth and metastasis. Overexpression of proangiogenic factors leads to uncontrolled vascular growth in tumors (T. Li et al., 2018). As a result, anti-angiogenic drugs are frequently used as a potential treatment option for cancer. Lectin-DyLight-649 combined with iDISCO presents a robust procedure for labeling the microvasculature in all areas in the body, including tumors. Changes in vessel density, tortuosity, and diameters can be quantified to evaluate the efficacy of novel anti-angiogenic treatments.

Ischemic strokes occur when there is a significant drop in cerebral blood flow due to occlusion in a cerebral artery. A major consequence of such an event is necrosis of neurons due to deficient blood supply (Datta et al., 2020). A method to visualize the microvascular network and the surrounding neurons, astrocytes, and glial cells can provide a detailed 3D snapshot of the brain in response to an ischemic stroke and monitor potential treatments over time.

In addition to visualizing cerebral microhemorrhages within the surrounding microvascular network and providing improved capability to estimate size range of these lesions, our approach can provide enhanced imaging for other disease entities. For example, a growing body of literature suggests a contribution of dysfunctional regulation of cerebral blood flow and various types of cognitive impairment (Sweeney et al., 2018). The ability to visualize the cerebral microvasculature in three dimensions offers a new gateway potentially leading to the identification of novel treatment targets for neurological disorders.

Disclosures

The authors do not have any competing interests to disclose.

Acknowledgements

This work was supported in part by the Arnold and Mabel Beckman Foundation and the National

Institutes of Health (Nos. T32HL116270, P41EB015890, R01NS020989, R21AG066000, R21NS111984, and 5TL1TR001415-07). This study was made possible in part through access to the Optical Biology Core Facility of the Developmental Biology Center, a shared resource supported by the Cancer Center Support Grant (CA-62203) and Center for Complex Biological Systems Support Grant (GM-076516) at the University of California, Irvine

Code, data, and materials availability

Data are available upon reasonable request to the corresponding author.

REFERENCES

Cai, R., Pan, C., Ghasemigharagoz, A., Todorov, M. I., Förstera, B., Zhao, S., Bhatia, H. S., Parra-Damas, A., Mrowka, L., Theodorou, D., Rempfler, M., Xavier, A. L. R., Kress, B. T., Benakis, C., Steinke, H., Liebscher, S., Bechmann, I., Liesz, A., Menze, B., … Ertürk, A. (2019). Panoptic imaging of transparent mice reveals whole-body neuronal projections and skull–meninges connections. *Nature Neuroscience*, *22*(2), 317–327. https://doi.org/10.1038/s41593-018-0301-3

Carmeliet, P., & Jain, R. K. (2011). Molecular mechanisms and clinical applications of angiogenesis. *Nature*, *473*(7347), 298–307. https://doi.org/10.1038/nature10144

Carrillo, M., Chuecos, M., Gandhi, K., Bednov, A., Moore, D. L., Maher, J., Ventolini, G., Ji, G., & Schlabritz-Loutsevitch, N. (2018). Optical tissue clearing in combination with perfusion and immunofluorescence for placental vascular imaging. *Medicine (United States)*, *97*(39), 10–13. https://doi.org/10.1097/MD.0000000000012392

Chung, K., Wallace, J., Kim, S. Y., Kalyanasundaram, S., Andalman, A. S., Davidson, T. J., Mirzabekov, J. J., Zalocusky, K. A., Mattis, J., Denisin, A. K., Pak, S., Bernstein, H., Ramakrishnan, C., Grosenick, L., Gradinaru, V., & Deisseroth, K. (2013). Structural and molecular interrogation of intact biological systems. *Nature*, *497*(7449), 332–337. https://doi.org/10.1038/nature12107

Crouzet, C., Jeong, G., Chae, R. H., LoPresti, K. T., Dunn, C. E., Xie, D. F., Agu, C., Fang, C., Nunes, A. C. F., Lau, W. L., Kim, S., Cribbs, D. H., Fisher, M., & Choi, B. (2021). Spectroscopic and deep learning-based approaches to identify and quantify cerebral microhemorrhages. *Scientific Reports*, *11*(1), 10725. https://doi.org/10.1038/s41598-021-88236-1

Datta, A., Sarmah, D., Mounica, L., Kaur, H., Kesharwani, R., Verma, G., Veeresh, P., Kotian, V., Kalia, K., Borah, A., Wang, X., Dave, K. R., Yavagal, D. R., & Bhattacharya, P. (2020). Cell Death Pathways in Ischemic Stroke and Targeted Pharmacotherapy. *Translational Stroke Research*, *11*(6), 1185–1202. https://doi.org/10.1007/s12975-020-00806-z

Di Giovanna, A. P., Tibo, A., Silvestri, L., Müllenbroich, M. C., Costantini, I., Allegra Mascaro, A. L., Sacconi, L., Frasconi, P., & Pavone, F. S. (2018). Whole-Brain Vasculature Reconstruction at the Single Capillary Level. *Scientific Reports*, *8*(1), 1–11. https://doi.org/10.1038/s41598-018-30533-3

Dice, L. R. (1945). Measures of the Amount of Ecologic Association Between Species. *Ecology*, *26*(3), 297–302.

Feng, L., Zhao, T., & Kim, J. (2015). neuTube 1.0: A New Design for Efficient Neuron Reconstruction Software Based on the SWC Format. *Eneuro*, *2*(1), ENEURO.0049-14.2014. https://doi.org/10.1523/ENEURO.0049-14.2014

Fu, Y. Y., & Tang, S. C. (2010). Optical clearing facilitates integrated 3D visualization of mouse ileal microstructure and vascular network with high definition. *Microvascular Research*, *80*(3), 512–521. https://doi.org/10.1016/j.mvr.2010.06.003

Gage, G. J., Kipke, D. R., & Shain, W. (2012). Whole animal perfusion fixation for rodents. *Journal of Visualized Experiments : JoVE*, *65*, 1–9. https://doi.org/10.3791/3564

Haller, S., Vernooij, M. W., Kuijer, J. P. A., Larsson, E. M., Jäger, H. R., & Barkhof, F. (2018). Cerebral microbleeds: Imaging and clinical significance. *Radiology*, *287*(1), 11–28. https://doi.org/10.1148/radiol.2018170803

Hama, H., Hioki, H., Namiki, K., Hoshida, T., Kurokawa, H., Ishidate, F., Kaneko, T., Akagi, T., Saito, T., Saido, T., & Miyawaki, A. (2015). ScaleS: An optical clearing palette for biological imaging. *Nature Neuroscience*, *18*(10), 1518–1529. https://doi.org/10.1038/nn.4107

Harrison, C. H., Buckland, G. R., Brooks, S. E., Johnston, D. A., Chatelet, D. S., Liu, A. K. L., Gentleman, S. M., Boche, D., & Nicoll, J. A. R. (2018). A novel method to visualise the three-dimensional organisation of the human cerebral cortical vasculature. *Journal of*

Anatomy, *232*(6), 1025–1030. https://doi.org/10.1111/joa.12805
Hart, W. E., Goldbaum, M., Côté, B., Kube, P., & Nelson, M. R. (1999). Measurement and classification of retinal vascular tortuosity. *International Journal of Medical Informatics*, *53*(2–3), 239–252. https://doi.org/10.1016/S1386-5056(98)00163-4
Huang, J., Brenna, C., Khan, A. ul M., Daniele, C., Rudolf, R., Heuveline, V., & Gretz, N. (2019). A cationic near infrared fluorescent agent and ethyl-cinnamate tissue clearing protocol for vascular staining and imaging. *Scientific Reports*, *9*(1), 1–13. https://doi.org/10.1038/s41598-018-36741-1
Ivins, S., Roberts, C., Vernay, B., & Scambler, P. J. (2016). Analysis of coronary vessels in cleared embryonic hearts. *Journal of Visualized Experiments*, *2016*(118), 1–9. https://doi.org/10.3791/54800
Jing, D., Zhang, S., Luo, W., Gao, X., Men, Y., Ma, C., Liu, X., Yi, Y., Bugde, A., Zhou, B. O., Zhao, Z., Yuan, Q., Feng, J. Q., Gao, L., Ge, W. P., & Zhao, H. (2018). Tissue clearing of both hard and soft tissue organs with the pegasos method. *Cell Research*, *28*(8), 803–818. https://doi.org/10.1038/s41422-018-0049-z
Kalaria, R. N., Akinyemi, R., & Ihara, M. (2016). Stroke injury, cognitive impairment and vascular dementia. *Biochimica et Biophysica Acta - Molecular Basis of Disease*, *1862*(5), 915–925. https://doi.org/10.1016/j.bbadis.2016.01.015
Khoradmehr, A., Mazaheri, F., Anvari, M., & Tamadon, A. (2019). A simple technique for three-dimensional imaging and segmentation of brain vasculature using fast free-of-acrylamide clearing tissue in murine. *Cell Journal*, *21*(1), 49–56. https://doi.org/10.22074/cellj.2019.5684
Khouri, K., Xie, D. F., Crouzet, C., Bahani, A. W., Cribbs, D. H., Fisher, M. J., & Choi, B. (2021). Simple methodology to visualize whole-brain microvasculature in three dimensions. *Neurophotonics*, *8*(02), 1–10. https://doi.org/10.1117/1.nph.8.2.025004
Kirst, C., Skriabine, S., Vieites-Prado, A., Topilko, T., Bertin, P., Gerschenfeld, G., Verny, F., Topilko, P., Michalski, N., Tessier-Lavigne, M., & Renier, N. (2020). Mapping the Fine-Scale Organization and Plasticity of the Brain Vasculature. *Cell*, *180*(4), 780-795.e25. https://doi.org/10.1016/j.cell.2020.01.028
Kolesová, H., Čapek, M., Radochová, B., Janáček, J., & Sedmera, D. (2016). Comparison of different tissue clearing methods and 3D imaging techniques for visualization of GFP-expressing mouse embryos and embryonic hearts. In *Histochemistry and Cell Biology* (Vol. 146, Issue 2, pp. 141–152). https://doi.org/10.1007/s00418-016-1441-8
Krolewski, D. M., Kumar, V., Martin, B., Tomer, R., Deisseroth, K., Myers, R. M., Schatzberg, A. F., Lee, F. S., Barchas, J. D., Bunney, W. E., Akil, H., & Watson, S. J. (2018). Quantitative validation of immunofluorescence and lectin staining using reduced CLARITY acrylamide formulations. *Brain Structure and Function*, *223*(2), 987–999. https://doi.org/10.1007/s00429-017-1583-z
Lagerweij, T., Dusoswa, S. A., Negrean, A., Hendrikx, E. M. L., de Vries, H. E., Kole, J., Garcia-Vallejo, J. J., Mansvelder, H. D., Vandertop, W. P., Noske, D. P., Tannous, B. A., Musters, R. J. P., van Kooyk, Y., Wesseling, P., Zhao, X. W., & Wurdinger, T. (2017). Optical clearing and fluorescence deep-tissue imaging for 3D quantitative analysis of the brain tumor microenvironment. *Angiogenesis*, *20*(4), 533–546. https://doi.org/10.1007/s10456-017-9565-6
Li, T., Kang, G., Wang, T., & Huang, H. (2018). Tumor angiogenesis and anti-angiogenic gene therapy for cancer (Review). In *Oncology Letters* (Vol. 16, Issue 1, pp. 687–702). https://doi.org/10.3892/ol.2018.8733
Li, Y., Song, Y., Zhao, L., Gaidosh, G., Laties, A. M., & Wen, R. (2008). Direct labeling and visualization of blood vessels with lipophilic carbocyanine dye DiI. *Nature Protocols*, *3*(11), 1703–1708. https://doi.org/10.1038/nprot.2008.172
Liebmann, T., Renier, N., Bettayeb, K., Greengard, P., Tessier-Lavigne, M., & Flajolet, M.

(2016). Three-Dimensional Study of Alzheimer's Disease Hallmarks Using the iDISCO Clearing Method. *Cell Reports*, *16*(4), 1138–1152. https://doi.org/10.1016/j.celrep.2016.06.060

Lo, P., Crouzet, C., Vasilevko, V., & Choi, B. (2016). Visualization of microbleeds with optical histology in mouse model of cerebral amyloid angiopathy. *Microvascular Research*, *105*, 109–113. https://doi.org/10.1016/j.mvr.2016.02.002

Loren, M., Crouzet, C., Bahani, A., Vasilevko, V., & Choi, B. (2019). Optical clearing potential of immersion-based agents applied to thick mouse brain sections. *PLoS ONE*, *14*(5), 1–14. https://doi.org/10.1371/journal.pone.0216064

Lugo-Hernandez, E., Squire, A., Hagemann, N., Brenzel, A., Sardari, M., Schlechter, J., Sanchez-Mendoza, E. H., Gunzer, M., Faissner, A., & Hermann, D. M. (2017). 3D visualization and quantification of microvessels in the whole ischemic mouse brain using solvent-based clearing and light sheet microscopy. *Journal of Cerebral Blood Flow and Metabolism*, *37*(10), 3355–3367. https://doi.org/10.1177/0271678X17698970

Matryba, P., Sosnowska, A., Wolny, A., Bozycki, L., Greig, A., Grzybowski, J., Stefaniuk, M., Nowis, D., & Gołąb, J. (2020). Systematic Evaluation of Chemically Distinct Tissue Optical Clearing Techniques in Murine Lymph Nodes. *The Journal of Immunology*, *204*(5), 1395–1407. https://doi.org/10.4049/jimmunol.1900847

McDonald, D. M. (2008). Angiogenesis and vascular remodeling in inflammation and cancer: Biology and architecture of the vasculature. *Angiogenesis: An Integrative Approach From Science to Medicine*, 17–33. https://doi.org/10.1007/978-0-387-71518-6_2

McKey, J., Cameron, L. A., Lewis, D., Batchvarov, I. S., & Capel, B. (2020). Combined iDISCO and CUBIC tissue clearing and lightsheet microscopy for in toto analysis of the adult mouse ovary. *Biology of Reproduction*, *102*(5), 1080–1089. https://doi.org/10.1093/biolre/ioaa012

Miyawaki, T., Morikawa, S., Susaki, E. A., Nakashima, A., Takeuchi, H., Yamaguchi, S., Ueda, H. R., & Ikegaya, Y. (2020). Visualization and molecular characterization of whole-brain vascular networks with capillary resolution. *Nature Communications*, *11*(1), 1–11. https://doi.org/10.1038/s41467-020-14786-z

Moy, A. J., Capulong, B. V., Saager, R. B., Wiersma, M. P., Lo, P. C., Durkin, A. J., & Choi, B. (2015). Optical properties of mouse brain tissue after optical clearing with FocusClear™. *Journal of Biomedical Optics*, *20*(9), 095010. https://doi.org/10.1117/1.jbo.20.9.095010

Moy, A. J., Lo, P. C., & Choi, B. (2014). High-resolution visualization of mouse cardiac microvasculature using optical histology. *Biomedical Optics Express*, *5*(1), 69. https://doi.org/10.1364/boe.5.000069

Moy, A. J., Wiersma, M. P., & Choi, B. (2013). Optical Histology: A Method to Visualize Microvasculature in Thick Tissue Sections of Mouse Brain. *PLoS ONE*, *8*(1), 2–9. https://doi.org/10.1371/journal.pone.0053753

Nehrhoff, I., Ripoll, J., Samaniego, R., Desco, M., & Gómez-Gaviro, M. V. (2017). Looking inside the heart: a see-through view of the vascular tree. *Biomedical Optics Express*, *8*(6), 3110. https://doi.org/10.1364/boe.8.003110

Nishimura, W., Sakaue-Sawano, A., Takahashi, S., Miyawaki, A., Yasuda, K., & Noda, Y. (2018). Optical clearing of the pancreas for visualization of mature β-cells and vessels in mice. In *Islets* (Vol. 10, Issue 3). https://doi.org/10.1080/19382014.2018.1451282

Oren, R., Fellus-Alyagor, L., Addadi, Y., Bochner, F., Gutman, H., Blumenreich, S., Dafni, H., Dekel, N., Neeman, M., & Lazar, S. (2018). Whole Organ Blood and Lymphatic Vessels Imaging (WOBLI). *Scientific Reports*, *8*(1), 1–9. https://doi.org/10.1038/s41598-018-19663-w

Peviani, M., Spano, G., Pagani, A., Brugnara, G., Covino, C., Galli, R., Biffi, A., & Politi, L. S. (2020). Lipophilic dye-compatible brain clearing technique allowing correlative magnetic resonance/high-resolution fluorescence imaging in rat models of glioblastoma. *Scientific*

Reports, *10*(1), 1–15. https://doi.org/10.1038/s41598-020-75137-y
Prabhakar, S., Lule, S., da Hora, C. C., Breakefield, X. O., & Cheah, P. S. (2021). Aav9 transduction mediated by systemic delivery of vector via retro-orbital injection in newborn, neonatal and juvenile mice. *Experimental Animals*, *70*(4), 450–458. https://doi.org/10.1538/expanim.20-0186
Qi, Y., Yu, T., Xu, J., Wan, P., Ma, Y., Zhu, J., Li, Y., Gong, H., Luo, Q., & Zhu, D. (2019). FDISCO: Advanced solvent-based clearing method for imaging whole organs. *Archivio Di Studi Urbani e Regionali*, *48*(122), 1–14. https://doi.org/10.1126/sciadv.aau8355
Renier, N., Wu, Z., Simon, D. J., Yang, J., Ariel, P., & Tessier-Lavigne, M. (2014). IDISCO: A simple, rapid method to immunolabel large tissue samples for volume imaging. *Cell*, *159*(4), 896–910. https://doi.org/10.1016/j.cell.2014.10.010
Ridler, T. W., & Calvard, S. (1978). Picture Thresholding Using An Interactive Selection Method. *IEEE Transactions on Systems, Man and Cybernetics*, *smc-8*(8), 630–632.
Robertson, R. T., Levine, S. T., Haynes, S. M., Gutierrez, P., Baratta, J. L., Tan, Z., & Longmuir, K. J. (2015). Use of labeled tomato lectin for imaging vasculature structures. *Histochemistry and Cell Biology*, *143*(2), 225–234. https://doi.org/10.1007/s00418-014-1301-3
Singh, J. N., Nowlin, T. M., Seedorf, G. J., Abman, S. H., & Shepherd, D. P. (2017). Quantifying three-dimensional rodent retina vascular development using optical tissue clearing and light-sheet microscopy. *Journal of Biomedical Optics*, *22*(07), 1. https://doi.org/10.1117/1.jbo.22.7.076011
Sumbria, R. K., Grigoryan, M. M., Vasilevko, V., Paganini-Hill, A., Kilday, K., Kim, R., Cribbs, D. H., & Fisher, M. J. (2018). Aging exacerbates development of cerebral microbleeds in a mouse model. *Journal of Neuroinflammation*, *15*(1), 1–7. https://doi.org/10.1186/s12974-018-1092-x
Susaki, E. A., Tainaka, K., Perrin, D., Kishino, F., Tawara, T., Watanabe, T. M., Yokoyama, C., Onoe, H., Eguchi, M., Yamaguchi, S., Abe, T., Kiyonari, H., Shimizu, Y., Miyawaki, A., Yokota, H., & Ueda, H. R. (2014). Whole-brain imaging with single-cell resolution using chemical cocktails and computational analysis. *Cell*, *157*(3), 726–739. https://doi.org/10.1016/j.cell.2014.03.042
Sweeney, M. D., Kisler, K., Montagne, A., Toga, A. W., & Zlokovic, B. V. (2018). The role of brain vasculature in neurodegenerative disorders. *Nature Neuroscience*, *21*(10), 1318–1331. https://doi.org/10.1038/s41593-018-0234-x
White, S. M., George, S. C., & Choi, B. (2011). Automated computation of functional vascular density using laser speckle imaging in a rodent window chamber model. *Microvascular Research*, *82*(1), 92–95. https://doi.org/10.1016/j.mvr.2011.03.006
Yardeni, T., Eckhaus, M., Morris, H. D., Huizing, M., & Hoogstraten-Miller, S. (2011). Retro-orbital injections in mice. *Lab Animal*, *40*(5), 155–160. https://doi.org/10.1038/laban0511-155
Yi, Y., Men, Y., Jing, D., Luo, W., Zhang, S., Feng, J. Q., Liu, J., Ge, W., Wang, J., & Zhao, H. (2019). 3-dimensional visualization of implant-tissue interface with the polyethylene glycol associated solvent system tissue clearing method. *Cell Proliferation*, *52*(3), e12578. https://doi.org/10.1111/cpr.12578
Zhu, D., Wang, J., Zhi, Z., Wen, X., & Luo, Q. (2010). Imaging dermal blood flow through the intact rat skin with an optical clearing method. *Journal of Biomedical Optics*, *15*(2), 026008. https://doi.org/10.1117/1.3369739
Zhu, J., Yu, T., Li, Y., Xu, J., Qi, Y., Yao, Y., Ma, Y., Wan, P., Chen, Z., Li, X., Gong, H., Luo, Q., & Zhu, D. (2020). MACS: Rapid Aqueous Clearing System for 3D Mapping of Intact Organs. *Advanced Science*, *7*(8), 1–14. https://doi.org/10.1002/advs.201903185